Theory of a two-step enantiomeric purification of racemic mixtures by optical means: The D_2S_2 molecule

Ioannis Thanopulos[a] and Petr Král
Department of Chemical Physics, The Weizmann Institute of Science, Rehovot, Israel

Moshe Shapiro
Department of Chemical Physics, The Weizmann Institute of Science, Rehovot, Israel, and the Departments of Chemistry and Physics, The University of British Columbia, Vancouver, Canada

(Received 11 April 2003; accepted 11 June 2003)

We present an optical ''enantio-purification switch'' that turns in two steps a racemic mixture of left-handed and right-handed chiral molecules into a pure sample containing the enantiomer of interest. The optical switch is composed of an ''enantio discriminator'' and an ''enantio converter'' acting in tandem. The method is robust, insensitive to decay processes, and does not require molecular preorientation. We demonstrate the method for the nanosecond purification of a racemate of (transiently chiral) D_2S_2 molecules. The energies of the rovibrational states and the related dipole elements are obtained by *ab initio* calculations. © *2003 American Institute of Physics.*
[DOI: 10.1063/1.1597491]

I. INTRODUCTION

The ''enantio separation'' of ''racemic'' mixtures (i.e., mixtures of enantiomers that are chiral molecules and their mirror images), is one of the most important and difficult problems in chemistry.[1–5] The even more ambitious task of converting the entire mixture into one enantiomer of choice (''enantio purification'') has also received much attention. The possibility of achieving this goal by purely optical means has been a topic of much interest in recent years.[6–16] In particular, this goal was shown to be realizable, using the strong electric–dipole photon coupling, by employing three (mutually perpendicular, linearly polarized) light beams in a method termed ''laser distillation.''[9–11] The laser distillation method, which involves the application of many cycles of optical excitation followed by relaxation,[9] was shown to be capable of gradually achieving enantio purification.

Our objective of the present paper is to show how this task can be performed in just two steps. Our method is based on a previous suggestion, according to which enantio separation (as distinct from enantio purification) could be achieved by a ''cyclic population transfer'' (CPT) process.[15] According to this approach, which is an extension of adiabatic passage (AP) phenomena,[17–19] one can separate enantiomers by executing an adiabatic population transfer process between three (e.g., rovibrational) quantum states, denoted as $|1\rangle$, $|2\rangle$, and $|3\rangle$. The method makes use of the fact that chiral molecules, which lack an inversion center, possess eigenstates of ill-defined parity. As a result, it is possible to execute simultaneously a one-photon transition $|1\rangle \rightarrow |3\rangle$ and a two-photon transition $|1\rangle \rightarrow |2\rangle \rightarrow |3\rangle$, thereby forming a ''loop'' or a ''cycle'' in which the two processes interfere. Simultaneously, the $|1\rangle \rightarrow |2\rangle$ process interferes with the $|1\rangle \rightarrow |3\rangle \rightarrow |2\rangle$ process.

The interference of these transitions renders CPT dependent on the total phase φ of the three Rabi frequencies (the product of the transition dipoles and the electric fields).[15,16] Since transition dipole matrix elements of the two enantiomers often differ in sign, the population evolution in the two enantiomers under the action of the three fields can be different. As a result, when both enantiomers initially occupy state $|1\rangle$, one enantiomer can be excited to state $|2\rangle$, while the other is transferred to state $|3\rangle$. By merely changing φ by π, one can exchange the enantiomer in state $|2\rangle$ with its mirror image in state $|3\rangle$. In this manner one can distinguish between the enantiomers and potentially separate them by, e.g., performing a selective ionization of the unwanted molecule.

The great advantage of the CPT scheme is that the separation process can be completed in just one step. Moreover, the process can take place solely on the ground electronic surface. In this way one can avoid disruptive competing processes, such as dissociation and internal conversion.[10] On the other hand, CPT is sensitive to variations in the lasers parameters, and, contrary to ''laser distillation,''[9] CPT leads to enantio separation but not to enantio purification (i.e., there is no conversion of one enantiomer into the other).

In this work, we present a robust extension of CPT called the ''enantio-purification switch,'' which can complete the purification of racemic mixtures by using optical pulses in two consecutive steps. In the first step, termed an ''enantio discriminator,'' we excite only one enantiomer, while leaving the other enantiomer in the mixture in its initial state. In the second step, called the ''enantio converter,'' the specific excited enantiomer is converted to its mirror image form. Thus, in just two steps, the racemic mixture of chiral molecules can be converted into the enantiomer of choice. Furthermore, the use of three mutually perpendicular polarizations during the first, enantio-discriminating step makes the prepolarization or preorientation of the molecules unnecessary.[11] The

[a]Electronic mail: ioannis@weizmann.ac.il

enantio-purification switch is demonstrated computationally for the (transiently chiral) D_2S_2 molecule.

This paper is organized as follows: Following our preliminary account,[16] the principles of the enantio discriminator are introduced in Sec. II, with D_2S_2 serving as an example. The principles of the ''enantio converter'' and the action of the ''enantio-purification switch'' on D_2S_2 are presented in Sec. III. Details of the *ab initio* calculations of the ground potential energy and electric dipole surfaces of D_2S_2, as well as the rovibrational eigenstates used, are presented in Sec. IV. Conclusions are drawn in Sec. V.

II. THE BASIC THEORY OF THE ENANTIO-DISCRIMINATOR

We consider a system composed of N molecular states $|i\rangle$ of energies ω_i (where atomic units, with $\hbar=1$, are used), being driven by an oscillating electric field,

$$\mathbf{E}(t)=\sum_{i\neq j}\mathcal{R}_e[\hat{\epsilon}_{i,j}\mathcal{E}_{i,j}(t)e^{-i\omega_{i,j}t}], \tag{1}$$

where $\hat{\epsilon}_{i,j}$ are the polarization directions of each field component and the $\omega_{i,j}$ frequencies are chosen to be in resonance with the $|i\rangle\leftrightarrow|j\rangle$ transition frequencies, i.e., $\omega_{i,j}\approx\omega_i-\omega_j$. With the Rabi frequencies defined as $\Omega_{i,j}(t)=\mu_{i,j}\mathcal{E}_{i,j}(t)$, where $\mu_{i,j}$ are the matrix elements of the transition-dipole component in the polarization direction, the Hamiltonian of the system in the rotating wave approximation is given as

$$H=\sum_{i=1}^{N}\omega_i|i\rangle\langle i|+\sum_{i>j=1}^{N}(\Omega_{i,j}(t)e^{-i\omega_{i,j}t}|i\rangle\langle j|+\text{H.c.}). \tag{2}$$

Expanding the system wave function as

$$|\psi(t)\rangle=\sum_{i=1}^{N}c_i(t)e^{-i\omega_i t}|i\rangle, \tag{3}$$

we obtain $\mathbf{c}=(c_1,c_2,\ldots,c_N)^T$ (^{T} denotes transpose), the (column) vector of the slow varying coefficients, as the solution of the matrix Schrödinger equation, $\dot{\mathbf{c}}(t)=-i\mathbf{H}(t)\cdot\mathbf{c}(t)$, with $\mathbf{H}(t)$ being the effective Hamiltonian matrix, whose explicit form is given for the enantio discriminator and the enantio converter below.

We now specialize the treatment to a pair of enantiomers. We assume a situation, depicted in Fig. 1 for D_2S_2, in which the ground electronic state contains two identical potential minima separated by a high barrier. At sufficiently low energies the molecular states appear as pairs $|i\rangle_D$ and $|i\rangle_L$ localized about the right (D) or left (L) potential minimum. If the barrier is sufficiently high, these states are degenerate and stationary, as they are practically identical in energy to the symmetric and antisymmetric true molecular energy eigenstates, denoted as $|i\rangle_S$ and $|i\rangle_A$, respectively, where

$$\begin{aligned}|i\rangle_S&=1/\sqrt{2}[|i\rangle_L+|i\rangle_D],\\ |i\rangle_A&=1/\sqrt{2}[|i\rangle_L-|i\rangle_D].\end{aligned} \tag{4}$$

As the energy gets higher the (tunneling) splitting between the $|i\rangle_S$ and $|i\rangle_A$ levels gets larger and larger and the $|i\rangle_{D,L}$ states cease to be stationary. Eventually the interconversion between the enantiomers becomes so facile and fast that it is more physical to work with the true energy eigenstates $|i\rangle_{S,A}$.

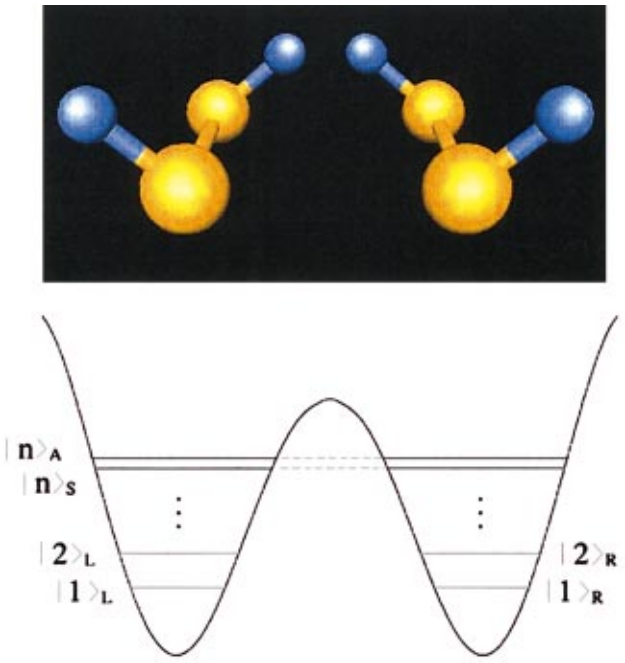

FIG. 1. (Color) The double well potential energy for the torsional motion of the D_2S_2 molecule. The two enantiomers connected by this stereo-mutation path are shown above their respective wells.

In the ''enantio-discriminator'' step, shown schematically in the upper plot of Fig. 2, we wish to separate the (racemic) mixture into the two enantiomers. Assuming that the two enantiomers are initially in a statistical mixture of

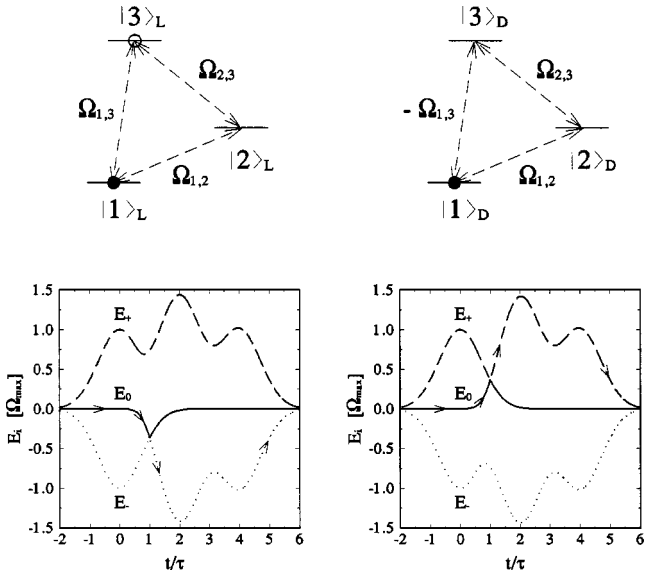

FIG. 2. (Upper plot) a schematic plot of the enantio discriminator. The three levels of each enantiomer are resonantly coupled by three fields. Particular dipole moments of the two enantiomers have opposite signs. (Lower plot) the time-dependence of the eigenvalues of the enentio discriminator. The population initially follows the $|E_0\rangle$ dark state. At $t\approx\tau_p$ the population crosses over diabatically to $|E_-\rangle$ for one enantiomer and to $|E_+\rangle$ for the other.

the $|1\rangle_{D,L}$ states, the task of the "discriminator" is to selectively transfer one enantiomer to the $|3\rangle$ state, while keeping the other enantiomer in the $|1\rangle$ state. This is a complicated task because, due to the near degeneracy of the $|i\rangle_L$ and the $|i\rangle_D$ levels for $i=1, 2, 3$, the driving light field $\mathbf{E}(t)$ simultaneously excites the same transitions in both enantiomers. Hence, we take advantage of the two CPT excitation loops,

$$|1\rangle_L \leftrightarrow |2\rangle_L \leftrightarrow |3\rangle_L \leftrightarrow |1\rangle_L ,$$
$$|1\rangle_D \leftrightarrow |2\rangle_D \leftrightarrow |3\rangle_D \leftrightarrow |1\rangle_D , \tag{5}$$

in which the two enantiomers are subjected to *different* interference conditions, and thus undergo *different* excitation, as we explain below.

The effective 3×3 Hamiltonian matrix of the enantio discriminator is given by

$$\mathbf{H}(t)=\begin{bmatrix} 0 & \Omega_{12}^*(t) & \Omega_{13}^*(t) \\ \Omega_{12}(t) & 0 & \Omega_{23}^*(t) \\ \Omega_{13}(t) & \Omega_{23}(t) & 0 \end{bmatrix}. \tag{6}$$

The overall enantio discriminator works as follows: the excitation process starts with a "dump" pulse $\mathcal{E}_{23}(t)$ that couples the $|2\rangle$ and $|3\rangle$ states. We choose the pulse such that the Rabi frequency has a form, $\Omega_{2,3}(t)=\Omega^{\max}f(t)$, where $f(t)=\exp[-t^2/\tau_p^2]$ with $\Omega_{\max}=1\,\mathrm{ns}^{-1}$. At this stage of the process all the population is in the adiabatic level $|E_0\rangle$. We next *simultaneously* add two "pump" pulses, of Rabi frequencies $\Omega_{12}(t)=\Omega_{13}(t)=\Omega_{\max}f(t-2\tau_p)$ that couple the $|1\rangle\leftrightarrow|2\rangle$ and the $|1\rangle\leftrightarrow|3\rangle$ states.

It turns out[15] that the difference in the dynamics of the D and L enantiomers with respect to the process of Eq. (5) arises from a difference in sign between the respective electric–dipole matrix elements, for a particular polarization of laser fields inducing the transition. This situation also occurs in D_2S_2, as shown in Table VI of Sec. IV, where its dipole moments for all transitions relevant to the enantiomeric switch are tabulated. The phase $\phi_{i,j}=\phi_{i,j}^{\mu}+\phi_{i,j}^{E}$ of each Rabi frequency $\Omega_{i,j}(t)$ is a sum of the (enantiospecific) phase of the $\mu_{i,j}=|\mu_{i,j}|e^{i\phi_{i,j}^{\mu}}$ dipole matrix element and the (common) phase of the electric field component $\mathcal{E}_{i,j}=|\mathcal{E}_{i,j}|e^{i\phi_{i,j}^{E}}$, resonant with the $i\rightarrow j$ transition. The total phase φ of the product of the three Rabi frequencies $\Omega_{i,j}(t)$, defined as $\varphi\equiv\phi_{1,2}+\phi_{2,3}+\phi_{3,1}$, and different in the two enantiomers, makes the D and L dynamics different.[15]

In order to understand this, we consider the time-dependent dressed adiabatic eigenstates $|E_-\rangle$, $|E_0\rangle$, and $|E_+\rangle$ of the Hamiltonian (6), depicted in the lower panel of Fig. 2. We obtain that at the particular time, $t=\tau_p$, when the three Rabi frequencies are equal, the $E_0(t)$ eigenvalue coincides with ("crosses") either the $E_+(t)$ or the $E_-(t)$ eigenvalue, depending on φ. Depending on the polarizations of the fields, one or all of the three Rabi frequencies $\Omega_{i,j}$ of the two enantiomers differ by a sign. This means in either case that $\varphi_D=\varphi_L+\pi$ and it follows that the eigenvalues crossing each other at $t=\tau_p$ are *different* for the two enantiomers.[15] At $t=\tau_p$, the system experiences *diabatic* dynamics and makes a smooth transition from the initially populated $|E_0\rangle$ eigenstate to either $|E_-\rangle$ or $|E_+\rangle$, depending on whether $\varphi=0$ or $\varphi=\pi$, i.e., on the identity of the enantiomer.

After the crossing is complete, at $t\gg\tau_p$, the eigenvalues separate and the dynamics become adiabatic again. The enantiomer population therefore remains confined to either $|E_-\rangle$ or $|E_+\rangle$. At this stage we slowly switch off the $\mathcal{E}_{1,2}(t)$ pulse while keeping the $\mathcal{E}_{1,3}(t)$ field on. Consequently, the zero adiabatic eigenstate $|E_0\rangle$ correlates adiabatically with state $|2\rangle$, which thus becomes *empty* after this process, while the occupied $|E_+\rangle$ and $|E_-\rangle$ states correlate to $|E_\pm\rangle\rightarrow(|1\rangle\pm|3\rangle)/\sqrt{2}$.

In order to complete the process, we modify $\Omega_{1,3}$, by adding to it a *chirped* component, of the form $f(t-4\tau_p)\exp\{-it\Omega^{\max}f(t-6\tau_p)\}$. Therefore, $\Omega_{1,3}$ assumes the form

$$\Omega_{1,3}(t)=\Omega^{\max}(f(t-2\tau_p)+f(t-4\tau_p)\times\exp\{-it\Omega^{\max}f(t-6\tau_p)\}). \tag{7}$$

The role of the chirped component in Eq. (7) is to adiabatically couple state $|1\rangle$ to state $|3\rangle$, since its action in the $\{|1\rangle,|3\rangle\}$ space is governed by an effective 2×2 Hamiltonian,

$$\mathbf{H}_{\mathrm{eff}}(t)=\Omega_{\max}\begin{bmatrix} f(t-6\tau_p)/2 & f(t-4\tau_p) \\ f(t-4\tau_p) & -f(t-6\tau_p)/2 \end{bmatrix}. \tag{8}$$

As a result of the chirp, at $t\approx5\tau_p$, the two eigenstates of $\mathbf{H}_{\mathrm{eff}}(t)$ change their nature adiabatically from the superposition state $(|1\rangle\pm|3\rangle)/\sqrt{2}$ to either $|1\rangle$ or $|3\rangle$, depending on whether $\varphi=0$ or $\varphi=\pi$. Due to the "$\pi/2$ rotation" induced by the chirped pulse, one enantiomer returns to the initial $|1\rangle$ state and the other switches over to the $|3\rangle$ state. We find the enantio discriminator to be a robust process, with all population transfer taking place smoothly without any oscillations.

In the laboratory implementation one envisions using a phase stabilized cw source at one of the frequencies of interest, say $\omega_{2,1}$, to seed a nonlinear crystal. Thus, given an $\omega_{2,3}$ pulse, the $\omega_{1,3}$ pulse will be generated (by sum-frequency or difference-frequency mixing), like in an OPA, in addition to the $\omega_{2,1}$ pulse. By introducing a phase delay element in the path of either one of these three pulses we can control the relative phase between them. Additionally, by changing the phase of the cw seed light we can make sure that the sum of the three phases (the "phase sum") of the three pulses is controllable.

Because it is not possible to say from *ab initio* theory which (D or L) enantiomer would be formed in the lab from a particular phase sum (this problem is akin to the fact that it is impossible to give an *ab initio* definition of the "right" and "left" concepts, and one must always use some standard to decide which is which), we must monitor the enantiomer formation; if we see that we are purifying the unwanted enantiomer, we then give a phase shift of π to the $\omega_{2,1}$ cw seed light in order to obtain the desired one.

This completes the discussion of the enantio discriminator, which separates the two enantiomers, by exciting one of them and leaving the other unexcited. We can, as in Ref. 15, be content with just that, but in order to go further and

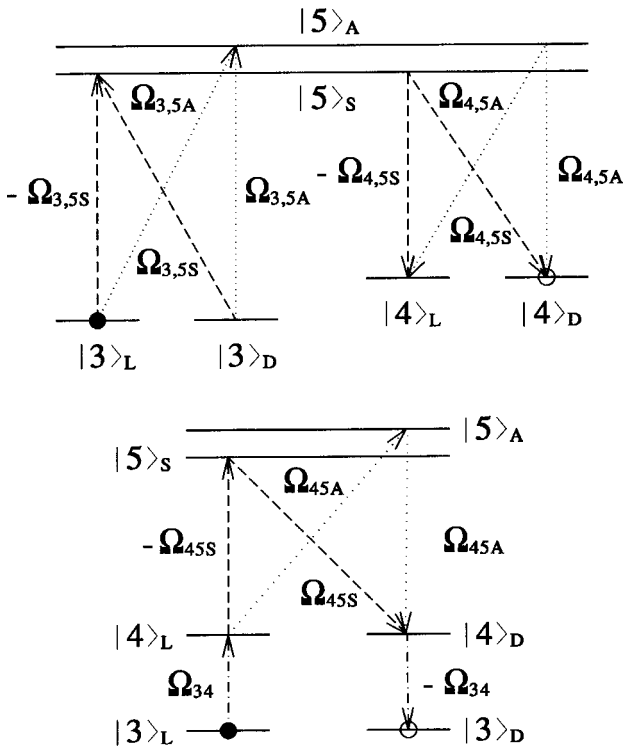

FIG. 3. (Upper plot) scheme *A* of the enantio converter: The population passes from the $|3\rangle_L$ state to the $|4\rangle_D$ state, while going through a superposition of the $|5\rangle_{S,A}$ states. (Lower plot) scheme *B* of the enantio converter: In the first transfer the population passes from the $|3\rangle_L$ state to the $|5\rangle_{S,A}$ states. In the second transfer, it passes from the $|5\rangle_{S,A}$ states to the $|3\rangle_D$ state.

achieve enantio purification,[16] we need to actively *convert* one enantiomer that has been thus separated to its mirror-imaged form, as we discuss in Sec. III.

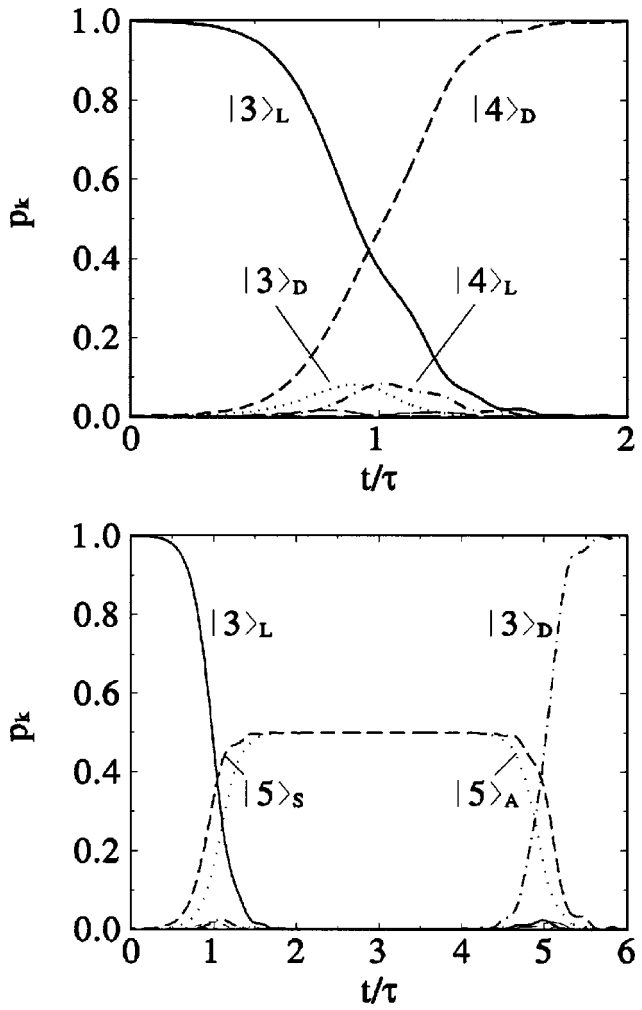

FIG. 4. (Upper plot) time dependence of the transitions in scheme *A* and (lower plot) in scheme *B* of the enantio converter.

III. THE ENANTIO CONVERTER

Assuming that the *L* enantiomer has been excited to the $|3\rangle_L$ state by the enantio-discriminator scheme, we now proceed to show how to convert it into a *D* enantiomer (in, say, the $|4\rangle_D$ state), while leaving the *D* enantiomer intact in the $|1\rangle_D$ state. We discuss the enantio-conversion strategy by two different schemes, *A* and *B*, shown in Fig. 3.

A. Scheme *A*

In this scheme, presented in Ref. 16, we perform the enantio conversion by creating a superposition of the well separated $|5\rangle_S$ and $|5\rangle_A$ states (see Table V). The "enantio-converter" process, a variation of a multipath transfer technique,[20] follows the path

$$|3\rangle_L \rightarrow \alpha e^{-i\omega_{5,S}t}|5\rangle_S + \beta e^{-i\omega_{5,A}t}|5\rangle_A \rightarrow |4\rangle_D, \tag{9}$$

schematically shown in the upper plot of Fig. 3.

The process starts with the application of two simultaneous "dump" pulses, $\mathcal{E}_{4,5S}(t)$ and $\mathcal{E}_{4,5A}(t)$, of duration $\tau_p \gg (\omega_{5,S}-\omega_{5,A})^{-1}$, which *resonantly* couple each of the $|5\rangle_S$ and $|5\rangle_A$ states to the $|4\rangle_L$ and $|4\rangle_D$ state. After a delay of $\sim 2\tau_p$, two "pump" pulses, $\mathcal{E}_{3,5S}(t)$ and $\mathcal{E}_{3,5A}(t)$, which resonantly couple each of the $|5\rangle_S$ and $|5\rangle_A$ states to the $|3\rangle_L$ and $|3\rangle_D$ states, are also introduced.

The used Rabi frequencies are $\Omega_{3,5S}(t)=\Omega^{\max} f(t-2\tau_p)$, $\Omega_{3,5A}(t)=0.5\,\Omega^{\max} f(t-2\tau_p)$, $\Omega_{4,5S}(t)=0.4\,\Omega^{\max} f(t)$ and $\Omega_{4,5A}(t)=-\Omega^{\max} f(t)$, with $\Omega^{\max}=30\,\mathrm{ns}^{-1}$ and $f(t)$ being identical to the function chosen for the discriminator, as discussed in Sec. II. Thus, the conversion of the excited enantiomer is achieved by choosing $\Omega_{4,5S}(t)$ to have the same sign as $\Omega_{3,5S}(t)$, and $\Omega_{4,5A}(t)$ to have the *opposite* sign to $\Omega_{3,5A}(t)$. This choice guarantees that states $|3\rangle_D$ and $|4\rangle_L$, which are nearly degenerate with the $|3\rangle_L$ and $|4\rangle_D$ states, respectively, are never populated. This result can be traced to the fact that with our choice of phases, the Rabi frequencies of the empty states, $|3\rangle_D$ and $|4\rangle_L$, form two *orthogonal*[20] vectors to the vectors of Rabi frequencies connected to states $|3\rangle_L$ and $|4\rangle_D$, respectively.

The evolution of the calculated populations $p_i=|c_i|^2$ is shown in the upper plot of Fig. 4. We see that indeed the process starts in the $|3\rangle_L$ state and ends in the $|4\rangle_D$ state. The states $|5\rangle_{S,A}$, although being absolutely necessary, never get actually populated during the process. As a result, the converter, and, in fact, the entire enantio-purification switch, is immune to dephasing processes that would otherwise destroy the coherence of the excited superposition state. For the same reason, the process would be unaffected by dissociation and/or internal conversion channels, arising otherwise when

the $|5\rangle_{S,A}$ states belong to an excited electronic state. A further discussion of the dynamics is presented in Ref. 16.

B. Scheme *B*

The "enantio converter" in scheme *B* is depicted in the lower plot of Fig. 3, for the first time. It is directly related to the method of Ref. 20, as does scheme *A*, but it uses a sequence of *two* two-photon steps,

$$|3\rangle_L \rightarrow |4\rangle_L \rightarrow |5\rangle, \quad |5\rangle \rightarrow |4\rangle_D \rightarrow |3\rangle_D . \tag{10}$$

In the first step, the population in the $|3\rangle_L$ state is transferred to the superposition state $|5\rangle = \alpha e^{-i\omega_{5S}t}|5\rangle_S + \beta e^{-i\omega_{5A}t}|5\rangle_A$. To this end, we simultaneously apply two "dump" pulses of Rabi frequencies $\Omega_{4,5S}(t)$ and $\Omega_{4,5A}(t)$ with duration $\tau_p \gg (\omega_{5S}-\omega_{5A})^{-1}$, which resonantly couple the $|4\rangle_L$ states to each of the $|5\rangle_S$ and $|5\rangle_A$ states. Then, we apply a single resonant "pump" pulse of Rabi frequency $\Omega_{3,4}(t)$, which couples states $|3\rangle_L$ and $|4\rangle_L$.

In the second two-photon step, the population in the superposition $|5\rangle$ state is transferred to the $|3\rangle_D$ state, by repeating this process with an *opposite* sequence of pulses. In order to achieve the handedness switching in the second ($|5\rangle \rightarrow |4\rangle_D$) step, the phase of the $\Omega_{4,5S(A)}(t)$ pulse is shifted by π relative to its value in the first ($|4\rangle_L \rightarrow |5\rangle$) step.

We expand the total wave function in a basis composed of six $|3_L\rangle$, $|4_L\rangle$, $|5_S\rangle$, $|5_A\rangle$, $|3_D\rangle$, $|4_D\rangle$ states. The vector of expansion coefficient is denoted as $\mathbf{c}(t) = (c_{3L}, c_{4L}, c_{5S}, c_{5A}, c_{3D}, c_{4D})$. Given this basis, the effective Hamiltonian matrix is given as

$$\mathbf{H}(t) = \begin{bmatrix} 0 & \Omega_{3,4} & 0 & 0 & 0 & 0 \\ \Omega_{3,4}^* & 0 & \Omega_{4,5S} & \Omega_{4,5A} & 0 & 0 \\ 0 & \Omega_{4,5S}^* & 0 & 0 & -\Omega_{4,5S} & 0 \\ 0 & \Omega_{4,5A}^* & 0 & 0 & \Omega_{4,5A} & 0 \\ 0 & 0 & -\Omega_{4,5S}^* & \Omega_{4,5A}^* & 0 & -\Omega_{3,4}^* \\ 0 & 0 & 0 & 0 & -\Omega_{3,4} & 0 \end{bmatrix}. \tag{11}$$

The Hamiltonian matrix has a similar form to other coupled STIRAP systems.[21]

As in the scheme *A*,[16] the Hamiltonian given by Eq. (11) has two zero and four nonzero $\pm\sqrt{|\Omega_{3,4}|^2 + 2|\Omega_{4,5S(A)}|^2}$ eigenvalues. The zero eigenvalues correspond to two dark states with the coefficients

$$\begin{aligned} \mathbf{c}_1(t) &= (-2\Omega_{4,5A}, 0, \Omega_{3,4}^*/r', \Omega_{3,4}^*, 0, 0), \\ \mathbf{c}_2(t) &= (0, 0, -\Omega_{3,4}^*, r'^*\Omega_{3,4}^*, 0, 0, 2\Omega_{4,5S}^*), \end{aligned} \tag{12}$$

with $r' = \Omega_{4,5S}/\Omega_{4,5A}$. Again, the system can follow two possible paths with final states of opposite handedness.

Assuming for simplicity that $r' = 1$, we have that in the beginning of the first step ($t = 0$), only the dark state given in terms of the $\mathbf{c}_1$ vector correlates with the initial state $|3\rangle_L$. At the end of the first step, the same dark state correlates with the $\mathbf{c}_1(t_{\text{end}}) = (0,0,1,1,0,0)$ vector; hence, at the end of the first step the final population resides in the $|5\rangle_S + |5\rangle_A$ state. In the second step ($|5\rangle \rightarrow |4\rangle_D \rightarrow |3\rangle_D$), we flip the phase of $\Omega_{4,5A}$ in order to have $r' = -1$. Now, the above state $\mathbf{c}_1(t_{\text{end}})$ correlates initially with the $\mathbf{c}_2$ dark state of the second step. Therefore, the population is transferred to $\mathbf{c}_2(t'_{\text{end}}) = (0,0,0,0,0,1)$, corresponding to the $|3\rangle_D$ state of opposite handedness to that of the initial state of the first step. The population transfer is robust with respect to variation of the magnitude of the ratio r', i.e., the system *bifurcates* between the two final states, similarly to the scheme *A*.

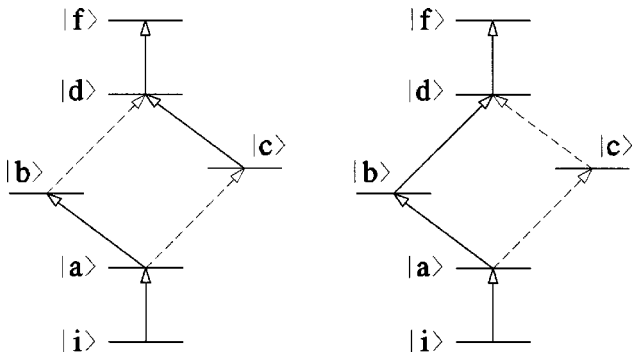

FIG. 5. (Left panel) the bifurcation scheme from Ref. 22. The absolute values of the Rabi frequencies are $\Omega_{ab} = \Omega_{cd} \neq \Omega_{ac} = \Omega_{bd}$ and $\Omega_{ia} = \Omega_{fd}$. (Right panel) the enantio converter scheme *B*, described above. Here the coupling strengths are $\Omega_{ab} = \Omega_{bd} \neq \Omega_{ac} = \Omega_{cd}$ and $\Omega_{ia} = \Omega_{fd}$.

We have performed simulations with the Rabi frequencies: $\Omega_{4,5S}(t) = \Omega^{\max}(f(t) - f(t-6\tau_p))$, $\Omega_{4,5A}(t) = 0.5\,\Omega^{\max}(f(t) + f(t-6\tau_p))$, $\Omega_{3,4}(t) = \Omega^{\max}(f(t-2\tau_p) + f(t-4\tau_p))$, with $f(t)$ and $\Omega^{\max}$ as in scheme *A*. Notice, the shift by π of the phase of the pump pulse $\Omega_{4,5S}(t)$, which is centered at $t = 6\tau_p$, in the second step.

The evolution of the p_i populations is shown in the lower plot of Fig. 4. We see that indeed a complete population transfer from the $|3\rangle_L$ to $|3\rangle_D$ state occurs by the sequence of events described above. We note that the populations of the $|5\rangle_{S,A}$ states are nearly the same, independent of the $\Omega_{4,5S}/\Omega_{4,5A}$ ratio of the Rabi frequencies. This is due to the symmetry of a six-level scheme with two pairs of degenerate *L*, *D* states.[21]

C. Comparison of two bifurcation schemes

The enantio converter of scheme *B*, schematically shown in Fig. 5 (right), is topologically equivalent to the six-level scheme[21] of Fig. 5 (left). It is interesting to discuss briefly the similarities and differences between these two schemes. The scheme of Ref. 21 (left panel) uses Rabi frequencies $\Omega_{ab} = \Omega_{cd} \neq \Omega_{ac} = \Omega_{bd}$. The population goes from the $|i\rangle$ state, via the $|a\rangle$ state, to either of the $|b\rangle$ or $|c\rangle$ states, depending on the Ω_{ab}/Ω_{ac} ratio of the Rabi frequencies. Notice that this transfer shows a bifurcation behavior, similar to that seen in schemes *A* and *B*. If we add another (delayed) time-reversed sequence of two pulses, the population transfer can continue to state $|f\rangle$ or return to state $|i\rangle$. In particular, if we switch the *ratio* $\Omega_{ab}/\Omega_{ac} = \Omega_{cd}/\Omega_{bd}$, the population *proceeds* to state $|f\rangle$ rather than proceeding to $|i\rangle$ for the former ratio.

On the right-hand panel, we show scheme *B* with $\Omega_{ab} = \Omega_{bd} \neq \Omega_{ac} = -\Omega_{cd}$. This scheme thus operates in the regime of instability of the scheme on the left-hand panel, with the important difference that in this case the elements in *one*

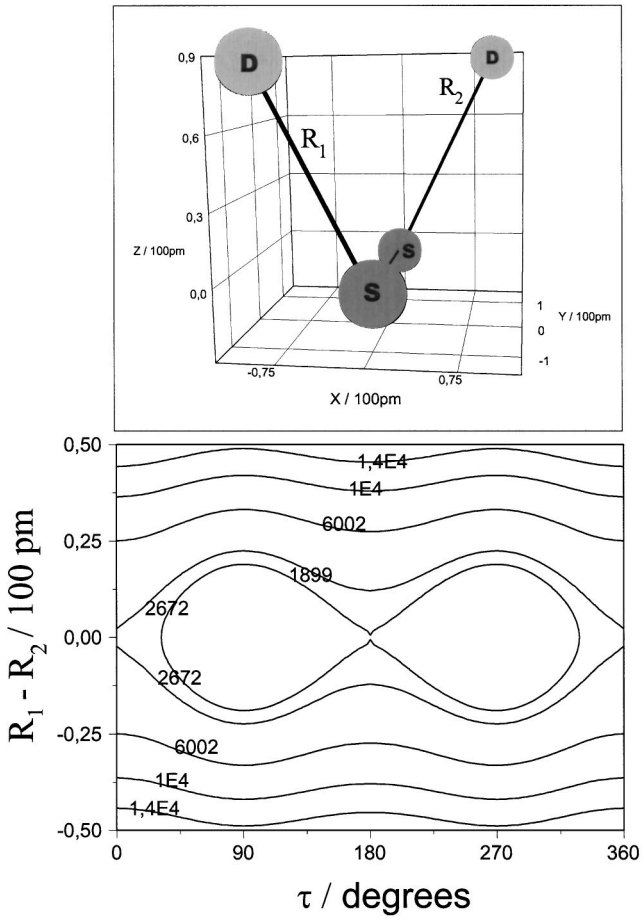

FIG. 6. The orientation of the D_2S_2 molecule fixed frame (upper part). Contour line plot of the two-dimensional potential energy surface including points with energy up to 14 000 cm^{-1} (lower part).

of the branches have an opposite sign ($\Omega_{ac}=-\Omega_{cd}$). As a result, the $|b\rangle$ or $|c\rangle$ states become equally populated at the end of the first transition, in contrast to the scheme on the left. On the other hand, if we add another sequence of pulses with reversed order, the population transfer can continue to state $|f\rangle$ or return to state $|i\rangle$, as the scheme of the left-hand panel. The population would *proceed* to state $|f\rangle$ if we switch the *signs* of the transition elements, $\Omega'_{ac}=-\Omega_{ac}$ and $\Omega'_{cd}=-\Omega_{cd}$ ($\Omega'_{ac}=-\Omega'_{cd}$). The population will *return* to the $|i\rangle$ state if the signs are kept unchanged. We thus see that these two schemes correspond to two regimes of evolution governed by the same topology.

IV. CALCULATIONS OF THE MOLECULAR ATTRIBUTES OF D_2S_2

In Fig. 1, we have shown the enantiomers of the (transiently chiral) D_2S_2 molecule, for which the enantio-purification switch is computationally demonstrated in Secs. II and III. In order to operate the switch in D_2S_2, we have used five pairs of rovibrational states, $\{1_L,1_D,2_L,2_D,3_L,3_D,4_L,4_D,5_S,5_A\}$, which we explicitly introduce in this section.

In Fig. 6 (up) we show the molecule with its molecule-fixed z axis oriented parallel to the principal axis with the smallest moment of inertia, conventionally named the c axis of the molecule, and the molecule-fixed y axis oriented parallel to the S–S bond. (We denote the molecule-fixed axes x, y, z by lowercase letters.)

D_2S_2 has six vibrational degrees of freedom, of which the large-amplitude torsional motion of the D atoms about the S–S bond is the relevant one for stereo mutation. According to our *ab initio* electronic structure calculations, which we present in detail below, there are two torsional stereo mutation barriers, one in the *cis* configuration and one in the *trans* configuration, whose heights are ~2700 and ~1900 cm^{-1}, respectively. D_2S_2 has C_2 symmetry at its equilibrium structure, but due to the possibility of tunneling through the two barriers, the use of the higher symmetry group $G_{2h}^{\dagger}$ for classifying the energy levels is required.[22,23] However, since the *cis* potential energy barrier is about 800 cm^{-1} higher than the *trans* barrier, we may consider it insuperable and use the approximate C_{2h} symmetry group instead of $G_{2h}^{\dagger}$.

A one-dimensional cut of the ground electronic potential energy surface along the stereo-mutation path over the *trans* barrier is shown in Fig. 1. The tunneling splitting of the lowest torsional level, which is not known experimentally, is predicted by our calculations to be $\sim 10^{-9}\,cm^{-1}$, corresponding to enantiomeric lifetime of 33 ms. Thus, although D_2S_2 is not a chiral molecule in the conventional sense, a molecular configuration described by superposition of the lowest torsional states, localized in one minimum of the double well potential, would stay chiral for sufficiently long times to be detected.

Optical transitions between the torsional D_2S_2 eigenstates, relevant to the stereo mutation, are induced only by the z component of the dipole moment. The existence of such transitions is, however, insufficient for the realization of the enantio-purification switch in D_2S_2 because, as we discuss below, transitions due to the x and y dipole moment components are also necessary.

It turns out that the antisymmetric S–D stretching mode allows, in general, for x and y transitions. Moreover, due to the large frequency difference between the torsion and the antisymmetric S–D stretching mode, it is reasonable to assume that their eigenstates are dynamically decoupled, at least for the lower-energy levels, which can be further used in our study. This assumption is supported by our results, as we discuss below. We therefore study the enantio-purification switch by explicitly considering the molecular configuration space of the torsional mode about the S–S bond and the S–D antisymmetric stretch.

A. *Ab initio* potential energy surface

We have calculated the potential energy surface of the configuration space as a function of two coordinates, one being the dihedral angle τ between the two DSS planes, describing the torsion around the S–S bond, and the other, $s \equiv R_1-R_2$, being the asymmetric S–D stretching motion. For this purpose, the coupled-cluster method including single and double excitations and a correction due to connected triple excitations, named CCSD(T)[24] has been used. The basis set employed is the correlated-consistent polarized

TABLE I. Absolute energy and optimized structural parameters for the equilibrium, the *cis* and the *trans* conformers of D_2S_2 (energy E in Hartree, bond lengths in Å, and angles in degrees). Harmonic frequencies (in cm^{-1}) at equilibrium are also presented. The assignments, with *st* referring to stretching and *b* to bending, are $\tilde{\nu}_1$=sym. *st* (S–D), $\tilde{\nu}_2$=sym. *b* (S–S–D), $\tilde{\nu}_3$ =*st* (D–D), $\tilde{\nu}_4$=torsion, $\tilde{\nu}_5$=asym. *st* (S–D), $\tilde{\nu}_6$=asym. *b* (S–S–D). Corresponding experimental values in parentheses.

τ	E	S–D	S–S	∠ (SSD)
0 (*cis*)	−796.659 439 5	1.3404	2.1387	95.8564
90.55 (equil.)	−796.671 479 1	1.3444	2.0825	97.7100
(90.34[a])		(1.3421[a])	(2.0564[a])	(97.88[a])
180 (*trans*)	−796.662 846 1	1.3413	2.1283	92.5574

Harmonic frequencies at equilibrium

$\tilde{\nu}_1$	1920.17	$\tilde{\nu}_4$	308.34(306[b])
$\tilde{\nu}_2$	647.45	$\tilde{\nu}_5$	1923.00(1863[b])
$\tilde{\nu}_3$	514.64	$\tilde{\nu}_6$	639.11

[a]From Ref. 28
[b]From Ref. 29.

basis, named *cc-pVTZ*,[25] with 96 contracted functions. All calculations have been performed using the GAUSSIAN 98 package.[26]

Calculations were carried out for a two-dimensional grid composed of 121 τ points ranging between $0° \leqslant \tau \leqslant 360°$ and 61 s points ranging as $-0.5\,\text{Å} \leqslant s \leqslant 0.5\,\text{Å}$. Due to the fact that only the first excited level of the asymmetric S–D stretching mode is used in the enantio-purification schemes, we avoid the computationally expensive full geometry optimization at the CCSD(T) level of theory for each $\{\tau,s\}$ point as follows: The energy profile for the $s=0$ minimum energy torsional path is fully relaxed with respect to all other coordinates; for $s\neq 0$ values, at each τ value, we increase one S–D bond length and decrease the other S–D bond length by the same amount (subjected to the $|s| \leqslant 0.5$ Å constraint), while keeping all other coordinates fixed at their $s=0$ (minimum energy path) relaxed values.

Although this procedure is expected to somewhat overestimate the asymmetric vibrational frequency, the enantio-purification switch is not sensitive to the particular value of this frequency. Moreover, the electric dipole moments obtained with the corresponding eigenfunctions should be minor influenced and it is expected to have practically no effect on the stereo-mutation dynamics due to the large frequency difference of the two modes. A contour plot of the two-dimensional potential energy surface is shown in Fig. 6 (down). It includes points up to 14 000 cm^{-1} above the potential energy minimum.

The *cis* and *trans* conformers of D_2S_2 correspond to $\tau=0$ and $\tau=180°$ at $s=0$, respectively. Table I presents the optimized bond lengths and bond angles for the equilibrated *cis* and *trans* molecular structures, showing good agreement with the experimental data.[28] The *ab initio* energies of all D_2S_2 conformers are also given in Table I. We find the *cis* barrier to be 2642 cm^{-1} and the *trans* barrier to be 1894 cm^{-1} above the potential energy minimum, while the experimental values are ~2800 and ~2000 cm^{-1}, respectively.[27]

Table I also contains the *ab initio* calculated harmonic frequencies at the equilibrium configuration for the six vibrational modes of D_2S_2, designated as follows: $\tilde{\nu}_1$ is the symmetric S–D stretching, $\tilde{\nu}_2$ is the symmetric S–S–D bending, $\tilde{\nu}_3$ is the D–D stretching, $\tilde{\nu}_4$ is the torsional mode, $\tilde{\nu}_5$ is the asymmetric S–D stretching, and $\tilde{\nu}_6$ is the asymmetric S–S–D bending mode. The only experimental data[29] known to us are tabulated in parentheses next to the corresponding *ab initio* values. The calculated torsional frequency is very close to the experimental value, in spite of the fact that torsion is a large-amplitude anharmonic motion.

TABLE II. Rotational eigenvalues E for $J=0$, 1, 2 for the asymmetric top D_2S_2 (in cm^{-1}) within the rigid rotor approximation, using the *ab initio* rotational constants.

J	K_aK_c	E	J	K_aK_c	E	J	K_aK_c	E
0	0 0	0.0	1	1 0	2.753 63	2	1 1	3.607 68
1	0 1	0.427 00	2	0 2	1.280 99	2	2 1	10.587 39
1	1 1	2.753 57	2	1 2	3.607 50	2	2 0	10.587 39

The *ab initio* rotational constants are (in GHz) $A_e = 76.150\,25$, $B_e = 6.401\,46$, and $C_e = 6.399\,61$, which imply an asymmetric parameter κ defined by[23]

$$\kappa \equiv \frac{2B_e - A_e - C_e}{A_e - C_e}, \tag{13}$$

of −0.999 946 9, as compared to the experimental value of $\kappa = -0.999\,999\,3$. Thus, D_2S_2 is an almost prolate symmetric top.

B. Rotational eigenstates

The rotational eigenstates are calculated within the rigid rotor approximation using parity adapted symmetric top eigenfunctions, defined by[11]

$$\mathbf{D}^{J,p}_{\lambda,M}(\phi,\theta,\chi) \equiv t_\lambda \sqrt{\frac{2J+1}{8\pi^2}} \left(D^J_{\lambda,M}(\phi,\theta,\chi) + p(-1)^\lambda D^J_{-\lambda,M}(\phi,\theta,\chi)\right). \tag{14}$$

Here, $\mathbf{D}^J_{\lambda,M}(\phi,\theta,\chi)$ are the rotational matrices,[30] where J is the total angular momentum, M is its projection on the laboratory Z axis (we use capital letters to denote the laboratory-fixed axes), and λ is its projection on the molecule-fixed z axis, $p=\pm 1$, $t_\lambda = 2^{-1/2}$ for $\lambda>0$ and $t_\lambda = 1/2$ for $\lambda=0$.

The rotational eigenvalues for $J=0$, 1, 2, using the asymmetric top K_a, K_c notation (K_a and K_c are the projection of the total angular momentum J on the a and c molecular principal axes), are given in Table II. We used the rotational constants obtained by our *ab initio* calculations. We find that the expansion of each asymmetric top eigenfunction $|J\,K_a\,K_c\rangle$ (where the M quantum number is suppressed) in terms of the parity adapted symmetric top eigenfunctions includes essentially only one $|\lambda|$. This fact further shows that D_2S_2 is essentially a prolate symmetric top. Thus, the $\mathbf{D}^{J,p}_{\lambda,M}$ functions of Eq. (14) approximate well the rotational eigenfunction of D_2S_2 (at least for the low J values studied here).

C. Vibrational eigenstates

The vibrational eigenstates are obtained using a Hamiltonian[31,32] for zero angular momentum, in terms of generalized vibrational coordinates $\{q_1,q_2,\ldots\}$ and generalized conjugate momenta $\{p_1,p_2,\ldots\}$, $p_j \equiv \partial_{q_j} \equiv -i\hbar\partial/\partial q_j$. It is given by

$$H(q_1,q_2,\ldots)=\tfrac{1}{2}\sum_{q_j,q_k}\partial_{q_j}G^{q_jq_k}(q_1,q_2,\ldots)\partial_{q_k} + u(q_1,q_2,\ldots)+V(q_1,q_2,\ldots). \quad (15)$$

Here, V is the potential energy and u is the "pseudopotential,"

$$u(q_1,q_2,\ldots)=\frac{\hbar^2}{8}\sum_{j,k}\frac{\partial}{\partial q_j}\left\{G_{jk}\frac{\partial \ln|\mathbf{g}|}{\partial q_k}\right\} + \frac{1}{4}\frac{\partial \ln|\mathbf{g}|}{\partial q_j}G_{jk}\frac{\partial \ln|\mathbf{g}|}{\partial q_k}, \quad (16)$$

where $|\mathbf{g}|$ is the determinant of the covariant vibrational metric tensor $\mathbf{g}$ given by

$$g_{jk}=\sum_a m_a\frac{\partial\vec{x}_a}{\partial q_j}\cdot\frac{\partial\vec{x}_a}{\partial q_k}. \quad (17)$$

In Eqs. (15), (16), $\mathbf{G}$ is the contravariant metric tensor, defined by

$$G^{q_1q_2}=\sum_a m_a^{-1}\frac{\partial q_1}{\partial\vec{x}_a}\cdot\frac{\partial q_2}{\partial\vec{x}_a}, \quad (18)$$

and related to $\mathbf{g}$ by

$$\mathbf{G}=(\mathbf{g}-\mathbf{C}^T\mathbf{I}^{-1}\mathbf{C})^{-1}. \quad (19)$$

Here, $\mathbf{C}$ denotes the Coriolis coupling matrix (^{T} stands for transpose) and $\mathbf{I}$ denotes the instantaneous tensor of inertia. The $\mathbf{I}$ and $\mathbf{C}$ matrices are given by

$$I_{\alpha\beta}=\sum_a m_a(\vec{e}_\alpha\times\vec{x}_a)\cdot(\vec{e}_\beta\times\vec{x}_a),$$
$$C_{\alpha j}=\sum_a m_a(\vec{e}_\alpha\times\vec{x}_a)\cdot\frac{\partial\vec{x}_a}{\partial q_j}. \quad (20)$$

In Eqs. (17)–(20), m_a is the mass of the ath atom in the molecule, $\vec{e}_\alpha$ ($\alpha=x,y,z$) are the unit vectors in the center-of-mass molecule-fixed frame, and $\vec{x}_a$ denotes the Cartesian coordinate vector of the ath atom in this frame.

We determine the vibrational eigenvalues using an equidistant discrete variable representation (Chebyshev-DVR)[33,34] of the two-dimensional Hamiltonian of Eq. (15), in the coordinates $\{\tau,s\}$. A computation of the above $\mathbf{g}$, $\mathbf{G}$, and u is performed using the Cartesian coordinates of the molecular structures in the two-dimensional configuration space. These coordinates are obtained from the bond lengths, bond angles, and dihedral angles and a "Z-matrix,"[35] i.e., a system of local polar coordinates widely used in quantum chemistry, e.g., in the GAUSSIAN programs.[26] The Z matrix was also used in previous studies[35–39] for the computation of the kinetic energy operator and the pseudopotential. The vibrational eigenstates obtained in the two-dimensional configuration space are labeled by $\{v_4,v_5\}$, where v_4 denotes the torsional and v_5 stands for the asymmetric S–D stretching mode quantum number, respectively. We always assume that the *cis* barrier is insuperable (C_{2h} symmetry) in our calculations, unless otherwise stated.

TABLE III. The $\tilde{\nu}_4$ and $\tilde{\nu}_5$ frequencies, obtained by two-dimensional and one-dimensional calculations, are presented, as well as the corresponding level splittings (in parentheses) induced by tunneling (C_{2h} symmetry). (See the text for a discussion.)

	2D		1D
{1,0}	**296.36**(2×10^{-7})	$\{v_4=1\}$	296.20(2×10^{-7})
{0,1}	**1945.74**(1×10^{-9})	$\{v_5=1\}$	1945.22

In order to understand better the dynamical coupling between the torsion and the asymmetric S–D stretching mode, we consider two cuts of the two-dimensional potential energy at $\tau=90.55°$ and $s=0$ Å, calculate the eigenstates in these two, one-dimensional subspaces, and compare the eigenvalues obtained in the two- and one-dimensional calculations. In the one-dimensional cases, we denote the eigenvalues by $\{v_5\}$ and $\{v_4\}$.

The energy values (in cm^{-1}) of levels with one torsional or one asymmetric S–D stretching quantum are given in Table III. The energies of the {1,0} and {0,1} states, calculated for the $\{\tau,s\}$ subspace, are tabulated in column "2D." In column "1D" we tabulate the $\{v_4\}$ and $\{v_5\}$ eigenvalues obtained from one-dimensional potential cuts at $s=0$ and at $\tau=90.55$, respectively. The corresponding tunneling splittings (in cm^{-1}) are given in parentheses. We see that the one- and two-dimensional results essentially coincide. This provides evidence that the asymmetric S–D stretching mode is only weakly coupled to the torsional motion, at least at the low-energy end of the spectrum.

Furthermore, in order to estimate the error incurred in the 2-D calculations, due to the fact that at $s\neq0$ the other degrees of freedom were not fully relaxed (they use relaxed values at $s=0$), we have repeated the *ab initio* calculation for a fully relaxed cut along the asymmetric S–D stretching coordinate s, in which the torsional angle was frozen at its equilibrium value of $\tau=90.55°$. Using the potential curve thus obtained, we have calculated the $\{v_5=1\}$ energy, which was found to be 1922.16 cm^{-1}. As expected, this value is lower than the {0,1} eigenvalue obtained in the partially relaxed calculations. It is essentially identical to the *ab initio* harmonic frequency of the v_5 mode (see Table I). From this we conclude that the {0,1} eigenvalue obtained from the partially relaxed 2-D potential surface is about 20 cm^{-1} higher than the fully relaxed value, representing a (minor) relative error of 1%.

We next focus on the pure torsional eigenstates ($v_5=0$), which are of primary interest to our enantiopurification calculations. Energy eigenvalues for such states are presented in Table IV. Results obtained within the two-dimensional subspace are compared with results using the torsional minimum energy path (one-dimensional potential

TABLE IV. Torsional energy eigenvalues E and splittings (in cm^{-1}) for the S and A components of the $v_4=0,...,5$ levels calculated in the two-dimensional potential surface [2-D (C_{2h}), only eigenstates with $v_5=0$] and in the one-dimensional potential energy cut at $s=0$ [1-D (C_{2h}) and 1-D ($G_{2h}^{\dagger}$)]. ΔE denotes the energy difference (in cm^{-1}) between the first two and the last two states of a torsional level (quartet) in the case of $G_{2h}^{\dagger}$ symmetry. (See the text for a discussion.)

v_4	S/A	2D (C_{2h})	1D (C_{2h})	1D ($G_{2h}^{\dagger}$)	
		E	E	E	ΔE
0	S	0.0	0.0	0.0	0.0
	A	(10^{-9})	(10^{-9})	(10^{-9})	0.0
1	S	296.3594	296.2046	296.2046	10^{-9}
	A	(2×10^{-7})	(2×10^{-7})	(2×10^{-7})	10^{-7}
2	S	579.5212	578.1195	578.1195	10^{-7}
	A	(10^{-5})	(10^{-5})	(2×10^{-5})	2×10^{-7}
3	S	848.4011	845.0467	845.0467	10^{-5}
	A	(6×10^{-4})[a]	(5×10^{-4})	(5×10^{-4})	10^{-5}
4	S	1101.4162	1095.7998	1095.7998	6×10^{-5}
	A	(2×10^{-2})	(2×10^{-2})	(2×10^{-2})	10^{-3}
5	S	1337.3960	1329.3639	1329.3634	5×10^{-4}
	A	(3.8×10^{-1})	(3.4×10^{-1})	(3.4×10^{-1})	3×10^{-3}

[a]Expt. value: 0.0003 cm^{-1} 41.

energy cut at $s=0$) for C_{2h} symmetry, as well as $G_{2h}^{\dagger}$ (allowing for tunneling through the *cis* barrier).

Within the C_{2h} symmetry group, each v_4 level has two components (doublet), with the energetically lower member labeled as S and the higher member labeled as A. In Table IV, we give the S member (given in cm^{-1} relative to the ground state) of the $v_4=0,...,5$ energy level doublets. In parentheses, we present the doublet splitting, i.e., the energy difference between the S and the A states in each doublet. Although the actual energies of the S members of the v_4 doublets obtained in the 2-D and 1-D calculations differ somewhat (especially for the higher v_4 values), the splittings of all the v_4 doublets coincide almost exactly in the two calculations. This fact is further evidence that the torsional mode is weakly coupled to the antisymmetric S–D mode at the low part of the spectrum.

We also briefly study the one-dimensional case, in which tunneling is allowed through the *cis* barrier ($G_{2h}^{\dagger}$ symmetry) and present the results in Table IV. Extending to $G_{2h}^{\dagger}$ symmetry, each S and A member of a v_4 doublet splits into two states, i.e., within $G_{2h}^{\dagger}$ symmetry each v_4 level consists of four closely spaced eigenstates (quartet). In this case we denote by S the lowest eigenstate of the lower doublet and by A the lowest eigenstate of the upper doublet of states within a v_4 quartet. The eigenvalues of the S and A states in all quartets are practically identical to the corresponding values obtained in the C_{2h} symmetry. Furthermore, the splitting in the lower or upper doublet of a quartet is always one order of magnitude smaller than the energy difference between the two doublets. A notable exception is the upper doublet of the $v_4=1$ quartet, for which the corresponding values are comparable, though very small in magnitude.

In the absence of experimental data for the tunneling splittings (except of the $v_4=3$ doublet; see Table IV), we can only compare our 1-D (C_{2h}) results with similar calculations.[40–41] However, only Ref. 41 reports results (which are in very good agreement with our calculations) of sufficient accuracy for this work.

D. Localized-chiral and delocalized-symmetry-adapted states

Two different proposals for the ''enantio-purification switch'' are introduced above. Both include five pairs of states given in Table V as a product of a vibrational part, $\{v_4,v_5\}$, and a rotational part, $|J,K_a,K_c,M\rangle$. However, the identity of some of them is different in the two schemes. In both schemes, chiral states, $|k_L\rangle$ and $|k_D\rangle$, defined as

$$|k\rangle_{L,D}=\frac{1}{\sqrt{2}}(|k\rangle_S\pm|k\rangle_A),\quad k=1,...,4, \tag{21}$$

for the first four pairs are used.

The $|k\rangle_L\leftrightarrow|k\rangle_D$ interconversion of states $k=1,...,3$ accompanying the corresponding tunneling splittings (see Table V) occurs within 33 ms–3.3 μs for scheme B and within 33–0.165 ms for scheme A. For $k=4$ this rate is 0.05

TABLE V. The five eigenstate pairs (C_{2h} symmetry) used in the enantio-purification schemes A and B, the energy of the corresponding lower symmetric component E_S with respect to the zero-point energy and the tunneling splitting $\Delta E_{S,A}$ for each pair. (Energy values are in cm^{-1}.)

$\|i\rangle$	v_4	v_5	J	K_aK_c	M	E_S	$\Delta E_{S,A}$	Scheme
$\|1\rangle$	0	0	0	0 0	0	0.0	10^{-9}	*A, B*
$\|2\rangle$	0	1	1	0 1	−1	1947.0583	10^{-9}	*A, B*
$\|3\rangle$	1	0	1	1 1	0	299.1130	2×10^{-7}	*B*
$\|3\rangle$	2	0	1	1 1	0	582.2748	10^{-5}	*A*
$\|4\rangle$	3	0	0	0 0	0	848.4011	6×10^{-4}	*A, B*
$\|5\rangle$	5	0	1	1 1	0	1340.1496	3.8×10^{-1}	*A, B*

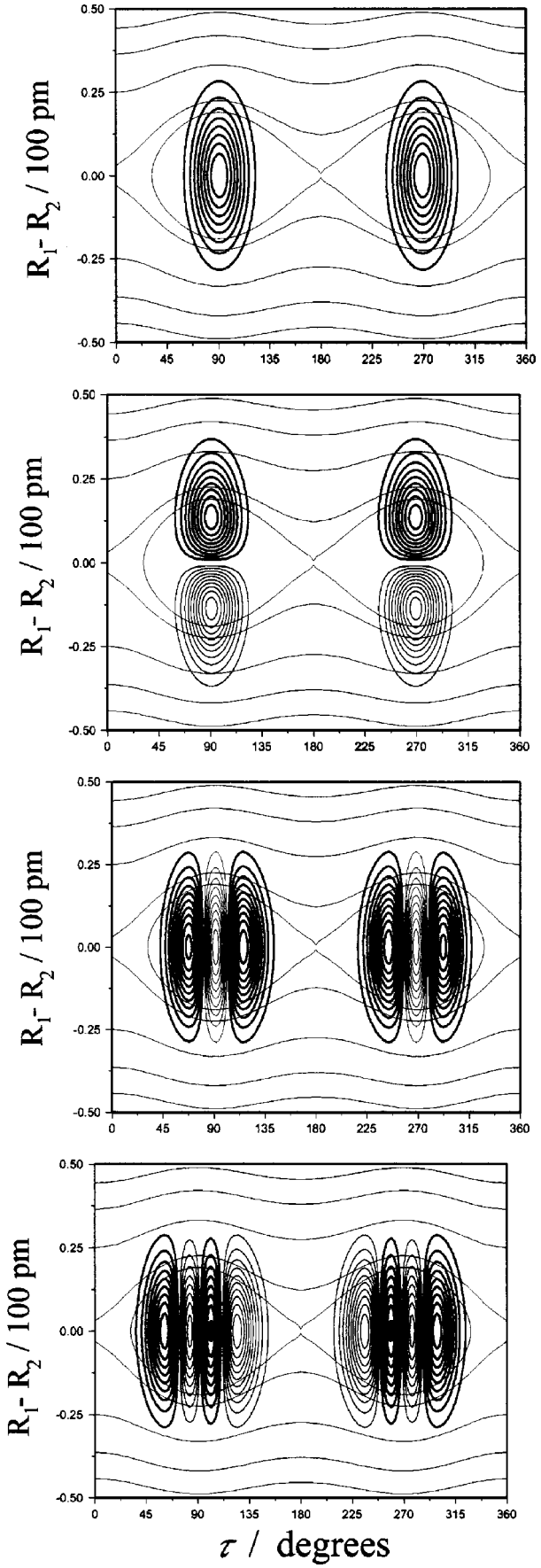

FIG. 7. The chiral $k=1,...,4$ vibrational wave functions (from top to bottom) in scheme *A*. Thin and thick lines denote negative and positive probability amplitudes, respectively.

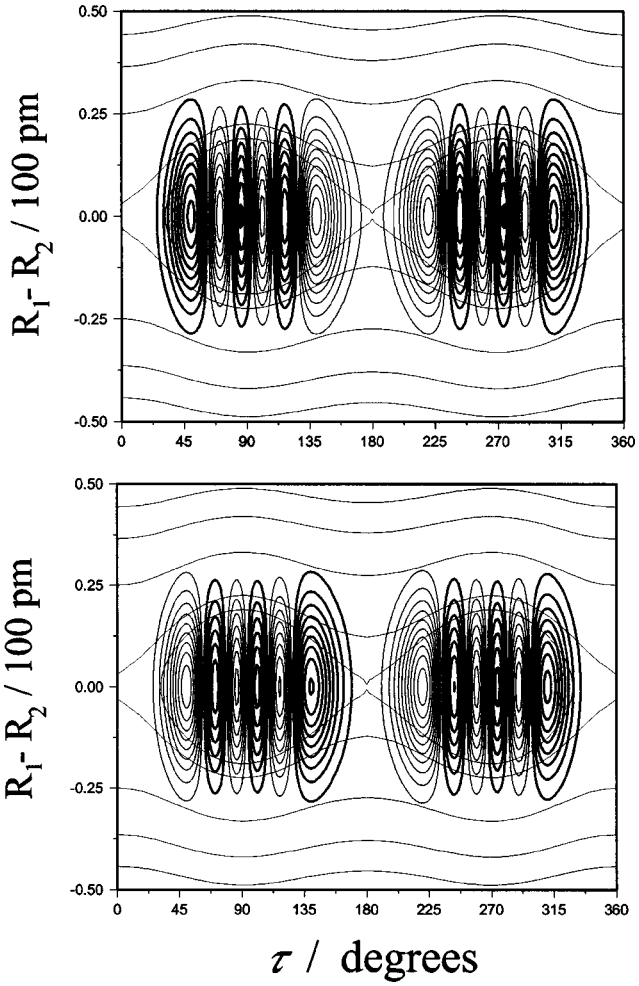

FIG. 8. The achiral *S* (upper part) and *A* (lower part) vibrational wave functions belonging to the fifth pair of states, common to schemes *A* and *B*. Thin and thick lines denotes negative and positive probability amplitude, respectively.

μs in both schemes. Thus, pulses of ns duration access both members of each of the $k=1,...,4$ doublets, thus justifying using the *L* and *D* states in our calculation.

The vibrational part of the states $|k\rangle_{L,D}$, $k=1,...,4$ used in scheme *A* are shown in Fig. 7 (from top to bottom). We see that indeed the *L* states are well localized on the left-hand ($\tau<180°$) part of the potential energy surface and the *D* states are well localized on the right ($\tau>180°$). On the other hand, the $|5\rangle_{S,A}$ states have the splitting $\Delta E^5_{S,A}=0.38\,\mathrm{cm}^{-1}$ and ns laser pulses should be separately tuned to each of them. These states are delocalized over the whole potential energy surface, as shown in Fig. 8.

On the basis of Table V, it is clear that use of the C_{2h} symmetry instead of the $G^{\dagger}_{2h}$ symmetry is totally justified, because the additional tiny splitting due to the possibility of tunneling through the *trans* barrier have no effect on the dynamics at the ns pulse durations considered. Further justification is also based on symmetry arguments.[27]

E. Electric dipole moment surface and matrix elements

At each point of the two-dimensional grid of the configuration space considered here, the electric dipole moment

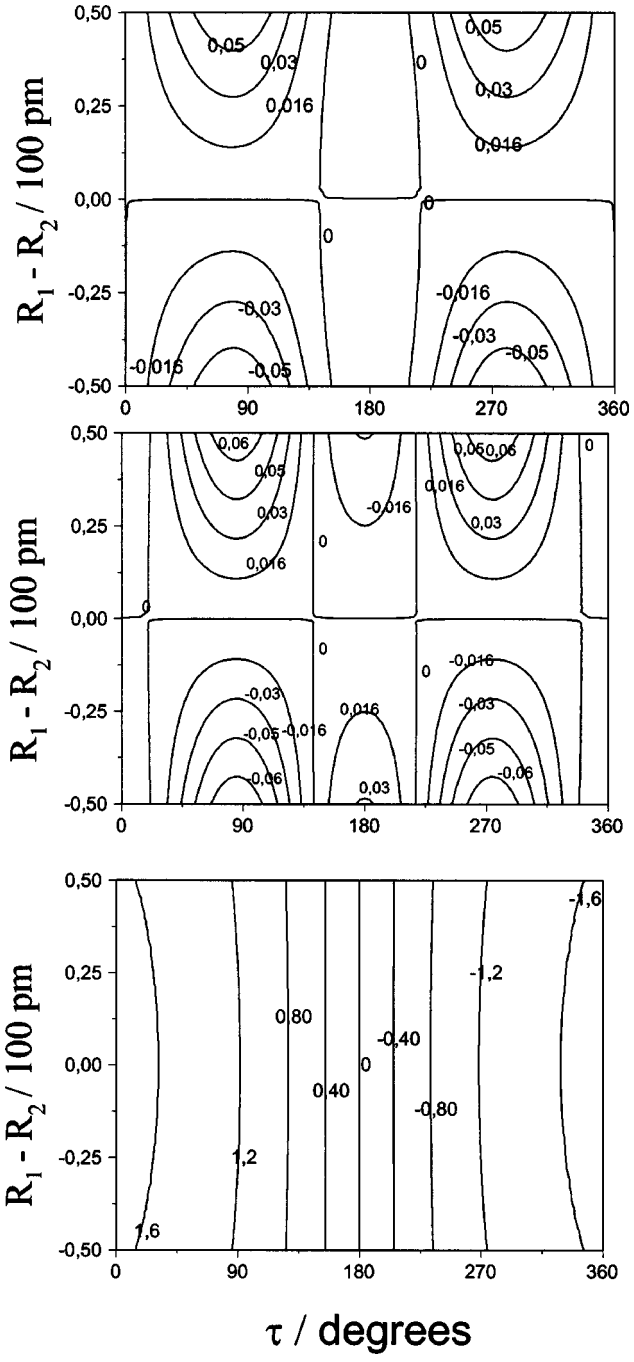

FIG. 9. Contour plots of the *x*, *y*, and *z* components (from top to bottom) of the electric dipole surface in the molecule-fixed frame.

of the corresponding molecular structure was calculated at the coupled-cluster level of theory, including only double excitations, CCD.[24] We have used the same basis set as in the potential energy surface calculations.

Contour plots of the *x*, *y*, and *z* components of the electric dipole in the molecule-fixed frame $\vec{\mu}_m$ are shown in Fig. 9. The *x* and *y* components are symmetric with respect to the torsional angle τ and antisymmetric with respect to *s*, while for the *z* component it is exactly opposite. The magnitude of the *z* component is usually one order of magnitude larger than the *x* and *y* components, leading to strong transitions between the torsional eigenstates.

TABLE VI. Nonvanishing laboratory-fixed electric dipole matrix elements μ_{ij}^{ℓ} ($\ell = X \pm iY, Z$) (in 10^{-3} Debye) used in our calculations. The relevant enantio-purification scheme (*A* or *B*) is given in parentheses.

$\mu^{X-iY}_{1_L 2_L}$	$\mu^{X+iY}_{2_L 3_L}$	$\mu^{Z}_{3_L 1_L}$	$\mu^{Z}_{3_L 4_L}$
$(-5-5\,i)\sqrt{2}(B)$	$(-0.3+0.3\,i)\sqrt{2}(B)$	55 (*B*)	9 (*B*)
$(-5-5\,i)\sqrt{2}(A)$	$(-0.3+0.3\,i)\sqrt{2}(A)$	3 (*A*)	
$\mu^{Z}_{4_L 5_S}$	$\mu^{Z}_{4_L 5_A}$	$\mu^{Z}_{3_L 5_S}$	$\mu^{Z}_{3_L 5_A}$
9 (*A*,*B*)	9 (*A*,*B*)	2 (*A*)	2 (*A*)
$\mu^{X-iY}_{1_D 2_D}$	$\mu^{X+iY}_{2_D 3_D}$	$\mu^{Z}_{3_D 1_D}$	$\mu^{Z}_{3_D 4_L}$
$(-5+5\,i)\sqrt{2}(B)$	$(-0.3-0.3\,i)\sqrt{2}(B)$	−55 (*B*)	−9 (*B*)
$(-5+5\,i)\sqrt{2}(A)$	$(-0.3-0.3\,i)\sqrt{2}(A)$	−3 (*A*)	
$\mu^{Z}_{4_D 5_S}$	$\mu^{Z}_{4_D 5_A}$	$\mu^{Z}_{3_D 5_S}$	$\mu^{Z}_{3_D 5_A}$
−9 (*A*,*B*)	9 (*A*,*B*)	−2 (*A*)	−2 (*A*)

Defining the laboratory axes to be oriented along three mutually perpendicular laser polarization directions, we obtain the electric dipole operator in the laboratory frame, μ_{ij}^{ℓ} ($\ell = X,Y,Z$),

$$\mu_{ij}^{X} = (\mu_{ij}^{-1} - \mu_{ij}^{1})/\sqrt{2}, \quad \mu_{ij}^{Y} = -i(\mu_{ij}^{-1} + \mu_{ij}^{1})/\sqrt{2}, \quad \mu_{ij}^{Z} = \mu_{ij}^{0}, \tag{22}$$

by transforming the electric dipole operator defined in the molecule-fixed frame,

$$\tilde{\mu}_{ij}^{(\pm 1)} = (\mp \tilde{\mu}_{ij}^{x} + i\tilde{\mu}_{ij}^{y})/\sqrt{2}, \quad \tilde{\mu}_{ij}^{0} = \tilde{\mu}_{ij}^{z}, \tag{23}$$

and using[30]

$$\mu_{ij}^{\rho} = \sum_{\sigma=-1,0,1} \tilde{\mu}_{ij}^{\sigma} D_{\rho,\sigma}^{1}(\phi,\theta,\chi), \quad \rho = -1,0,1, \tag{24}$$

where $D_{\rho,\sigma}^{1}(\phi,\theta,\chi)$ are the rotational matrices for $J=1$, as defined by Edmonds.[30]

The μ_{ij}^{ℓ} ($\ell = X,Y,Z$) dipole matrix elements used in all calculations are given in Table VI. They are calculated using the wave functions of the corresponding rovibrational states obtained as discussed above and the dipole operators given by Eq. (22). In Table VI it is shown that the transitions in the enantio discriminator are induced by three mutually perpendicular linearly polarized fileds. This is needed in order to obtain a closed loop of transitions starting from the ground rovibrational state of D_2S_2. We, thus, also avoid deleterious averaging of the angular momentum directions.[11] Finally, all transitions in the enantio-converter schemes *A* and *B* are induced by the *Z* component of the dipole moment.

V. CONCLUSIONS

We have presented a two-step optical enantio-purification switch, composed of an enantio discriminator and an enantio converter. In the enantio-discriminator step, only one enantiomer is excited, depending on the phase of the laser fields used. In the enantio-converter step, this particular enantiomer excited is converted to its mirror-imaged form. In this way an entire racemic mixture can be converted to a single enantiomer.

The process is robust with respect to the laser parameters. The main requirement in the presence of collisions with an environment is for the duration of the laser pulses to be shorter than the T_2 dephasing and T_1 collisional relaxation times. With the ns laser pulses considered here, this is usually the case in the gas phase.

We have only considered purifying low-temperature racemic mixtures for which only the lowest rovibrational state of each enantiomer is being populated. One can also purify racemic mixtures at higher temperatures, where more states are initially populated by repeating the present enantio-purification scheme several times. The depletion of a single state of a given enantiomer will cause, due to thermal equilibration, other states of the same enantiomer to be depleted. After several applications of this enantio-purification switch the entire thermal population of one enantiomer will be converted to the other.

ACKNOWLEDGMENTS

We acknowledge discussions with E. Frishman and P. Brumer. This project was supported by the Minerva Foundation, GIF, the EU IHP program HPRN-CT-1999-00129, the Office of Naval Research, and the Swiss Friends of the Weizmann Institute.

[1] W. S. Knowles Nobel lecture, 2001; Angew. Chem., Int. Ed. Engl. **41**, 1997 (2002).
[2] K. Bodenhöfer, A. Hierlemann, J. Seemann *et al.*, Nature (London) **387**, 577 (1997).
[3] R. McKendry, M.-E. Theoclitou, T. Rayment, and C. Abell, Nature (London) **391**, 566 (1998).
[4] M. Quack, Angew. Chem., Int. Ed. Engl. **28**, 571 (1989).
[5] H. Zepik, E. Shavit, M. Tang *et al.*, Science **295**, 1266 (2002).
[6] M. Shapiro and P. Brumer, J. Chem. Phys. **95**, 8658 (1991).
[7] C. S. Maierle and R. A. Harris, J. Chem. Phys. **109**, 3713 (1998).
[8] A. Salam and W. J. Meath, Chem. Phys. **228**, 115 (1998).
[9] M. Shapiro, E. Frishman, and P. Brumer, Phys. Rev. Lett. **84**, 1669 (2000).
[10] D. Gerbasi, M. Shapiro, and P. Brumer, J. Chem. Phys. **115**, 5349 (2001).
[11] E. Frishman, M. Shapiro, D. Gerbasi, and P. Brumer, J. Chem. Phys. (to be published).
[12] P. Brumer, E. Frishman, and M. Shapiro, Phys. Rev. A **65**, 015401 (2001).
[13] Y. Fujimura, L. Gonzalez, K. Hoki, J. Manz, and Y. Ohtsuki, Chem. Phys. Lett. **306**, 1 (1999); **310**, 578 (1999); Y. Fujimura, L. Gonzalez, K. Hoki, D. Kroener, J. Manz, and Y. Ohtsuki, Angew. Chem., Int. Ed. Engl. **39**, 4586 (2000); K. Hoki, Y. Ohtsuki, and Y. Fujimura, J. Chem. Phys. **114**, 1575 (2001); K. Hoki, D. Kroener, and J. Manz, Chem. Phys. **267**, 59 (2001); K. Hoki, L. Gonzalez, and Y. Fujimura, J. Chem. Phys. **116**, 8799 (2002).
[14] K. Hoki, L. Gonzalez, and Y. Fujimura, J. Chem. Phys. **116**, 2433 (2002); Y. Ohta, K. Hoki, and Y. Fujimura, *ibid.* **116**, 7509 (2002); L. Gonzalez, D. Kroener, and I. R. Sola, *ibid.* **115**, 2519 (2001).
[15] P. Král and M. Shapiro, Phys. Rev. Lett. **87**, 183002 (2001).
[16] P. Král, I. Thanopulos, M. Shapiro, and D. Cohen, Phys. Rev. Lett. **90**, 033001 (2003).
[17] D. Grischkowsky and M. M. T. Loy, Phys. Rev. A **12**, 1117 (1975); **12**, 2514 (1975).
[18] J. Oreg, F. T. Hioe, and J. H. Eberly, Phys. Rev. A **29**, 690 (1984).
[19] U. Gaubatz, P. Rudecki, S. Schiemann, and K. Bergmann, J. Chem. Phys. **92**, 5363 (1990); for a review, see K. Bergmann, H. Theuer, and B. W. Shore, Rev. Mod. Phys. **70**, 1003 (1998).
[20] P. Král, Z. Amitay, and M. Shapiro, Phys. Rev. Lett. **89**, 063002 (2002).
[21] P. Král, J. Fiurášek, and M. Shapiro, Phys. Rev. A **64**, 023414 (2001).
[22] J. T. Houghen, Can. J. Phys. **64**, 1392 (1984).
[23] P. R. Bunker and P. Jensen, *Molecular Symmetry and Spectroscopy*, 2nd ed. (NRC Research Press, Ottawa, 1998).
[24] K. Raghavachari, G. W. Trucks, J. A. Pople, and M. Head-Gordon, Chem. Phys. Lett. **157**, 479 (1989); G. E. Scuseria and T. J. Lee, J. Chem. Phys. **93**, 5851 (1990).
[25] T. H. Dunning, Jr., Chem. Phys. **90**, 1007 (1989); D. E. Woon and T. H. Dunning, Jr., J. Chem. Phys. **98**, 1358 (1993).
[26] M. J. Frisch, G. W. Trucks, H. B Schlegel *et al.*, GAUSSIAN 98, Revision A.11, Gaussian, Inc., Pittsburgh, PA, 2001.
[27] S. Urban, E. Herbst, P. Mittler, G. Winnewisser, K. M. Y. Yamada, and M. Winnewisser, J. Mol. Spectrosc. **137**, 327 (1989).
[28] J. Behrend, P. Mittler, G. Winnewisser, and K. M. T. Yamada, J. Mol. Spectrosc. **150**, 99 (1991).
[29] B. P. Winnewisser and M. Winnewisser, Z. Naturforsch. A **23**, 832 (1968).
[30] A. R. Edmonds, *Angular Momentum in Quantum Mechanics*, 2nd ed. (Princeton University Press, Princeton, NJ, 1960).
[31] R. Mayer and H. H. Günthard, J. Chem. Phys. **49**, 1510 (1968); **50**, 353 (1970).
[32] M. A. Hartchcock and J. Laane, J. Phys. Chem. **89**, 4231 (1985).
[33] D. T. Colbert and W. H. Miller, J. Chem. Phys. **96**, 1982 (1992).
[34] J. C. Light and T. Carrington, Jr., Adv. Chem. Phys. **114**, 263 (2000).
[35] D. Lauvergnat and A. Nauts, J. Chem. Phys. **116**, 8560 (2002).
[36] R. Meyer, J. Mol. Spectrosc. **76**, 266 (1979).
[37] M. L. Senent, Chem. Phys. Lett. **296**, 299 (1998).
[38] D. Luckhaus, J. Chem. Phys. **113**, 1329 (2000).
[39] G. Winnewisser, Vib. Spectrosc. **8**, 241 (1995).
[40] M. L. Senent, Y. G. Smeyers, R. Domiguez-Gomez, A. Arroyo, and S. Fernandez-Herrera, J. Mol. Spectrosc. **203**, 209 (2000).
[41] M. Gottselig, D. Luckhaus, M. Quack, J. Stohner, and M. Willeke, Helv. Chim. Acta **84**, 1846 (2000).